Research Article | Vol. 26, No. 12 | 11 Jun 2018 | OPTICS EXPRESS 15726
Optics EXPRESS

Temperature stability of thin film refractory plasmonic materials

MATTHEW P. WELLS,[1] RYAN BOWER,[1] REBECCA KILMURRAY,[1] BIN ZOU,[1] ANDREI P. MIHAI,[1] GOMATHI GOBALAKRICHENANE,[2] NEIL MCN. ALFORD,[1] RUPERT F. M. OULTON,[3] LESLEY F. COHEN,[3] STEFAN A. MAIER,[3,4] ANATOLY V. ZAYATS,[5] AND PETER K. PETROV[1,*]

[1]*Department of Materials, Imperial College London, Prince Consort Road, London SW7 2BP, UK*
[2]*Polytech Paris UPMC, 4 Place Jussieu, 75005 Paris, France*
[3]*Department of Physics, Imperial College London, Prince Consort Road, London SW7 2AZ, UK*
[4]*Faculty of Physics, Ludwig-Maximilians-Universität München, 80799 München, Germany*
[5]*Department of Physics, King's College London, Strand, London WC2R 2LS, UK*
[*]*p.petrov@imperial.ac.uk*

Abstract: Materials such as W, TiN, and $SrRuO_3$ (SRO) have been suggested as promising alternatives to Au and Ag in plasmonic applications owing to their stability at high operational temperatures. However, investigation of the reproducibility of the optical properties after thermal cycling between room and elevated temperatures is so far lacking. Here, thin films of W, Mo, Ti, TiN, TiON, Ag, Au, $SrRuO_3$ and $SrNbO_3$ are investigated to assess their viability for robust refractory plasmonic applications. These results are further compared to the performance of $SrMoO_3$ reported in literature. Films ranging in thickness from 50 to 105 nm are deposited on MgO, $SrTiO_3$ and Si substrates by e-beam evaporation, RF magnetron sputtering and pulsed laser deposition, prior to characterisation by means of AFM, XRD, spectroscopic ellipsometry, and DC resistivity. Measurements are conducted before and after annealing in air at temperatures ranging from 300 to 1000° C for one hour, to establish the maximum cycling temperature and potential longevity at elevated temperatures for each material. It is found that $SrRuO_3$ retains metallic behaviour after annealing at 800° C, while $SrNbO_3$ undergoes a phase transition resulting in a loss of metallic behaviour after annealing at 400° C. Importantly, the optical properties of TiN and TiON are degraded as a result of oxidation and show a loss of metallic behaviour after annealing at 500° C, while the same is not observed in Au until annealing at 600° C. Nevertheless, both TiN and TiON may be better suited than Au or SRO for high temperature applications operating under vacuum conditions.

Published by The Optical Society under the terms of the Creative Commons Attribution 4.0 License. Further distribution of this work must maintain attribution to the author(s) and the published article's title, journal citation, and DOI.

OCIS codes: (160.0160) Materials; (310.0310) Thin films; (250.5403) Plasmonics.

References and links

1. D. K. Gramotnev and S. I. Bozhevolnyi, "Plasmonics beyond the diffraction limit," Nat. Photonics **4**(2), 83–91 (2010).
2. U. Guler, V. M. Shalaev, and A. Boltasseva, "Nanoparticle plasmonics: going practical with transition metal nitrides," Mater. Today **18**(4), 227–237 (2015).
3. A. V. Krasavin and A. V. Zayats, "Active Nanophotonic Circuitry Based on Dielectric□loaded Plasmonic Waveguides," Adv. Opt. Mat. **3**(12), 1662–1690 (2015).
4. K. F. MacDonald and N. I. Zheludev, "Active plasmonics: current status," Laser Photonics Rev. **4**(4), 562–567 (2010).
5. S. Pillai and M. A. Green, "Plasmonics for photovoltaic applications," Sol. Energy Mater. Sol. Cells **94**(9), 1481–1486 (2010).
6. G. V. Naik, V. M. Shalaev, and A. Boltasseva, "Alternative plasmonic materials: beyond gold and silver," Adv. Mater. **25**(24), 3264–3294 (2013).
7. P. B. Johnson and R. W. Christy, "Optical constants of the noble metals," Phys. Rev. B **6**(12), 4370–4379 (1972).

#326055 https://doi.org/10.1364/OE.26.015726
Journal © 2018 Received 16 Mar 2018; revised 1 May 2018; accepted 1 May 2018; published 7 Jun 2018

Optics EXPRESS

8. A. Boltasseva, "Empowering plasmonics and metamaterials technology with new material platforms," MRS Bull. **39**(5), 461–468 (2014).
9. G. Albrecht, S. Kaiser, H. Giessen, and M. Hentschel, "Refractory Plasmonics without Refractory Materials," Nano Lett. **17**(10), 6402–6408 (2017).
10. H. Reddy, U. Guler, A. V. Kildishev, A. Boltasseva, and V. M. Shalaev, "Temperature dependent optical properties of gold thin films," Opt. Mater. Express **6**(9), 2776–2802 (2016).
11. N. P. Harder and P. Würfel, "Theoretical limits of thermophotovoltaic solar energy conversion," Semicond. Sci. Technol. **18**(5), S151–S157 (2003).
12. S. Molesky, C. J. Dewalt, and Z. Jacob, "High temperature epsilon-near-zero and epsilon-near-pole metamaterial emitters for thermophotovoltaics," Opt. Express **21**(S1), A96–A110 (2013).
13. Y. Nam, Y. X. Yeng, A. Lenert, P. Bermel, I. Celanovic, M. Soljačić, and E. N. Wang, "Solar thermophotovoltaic energy conversion systems with two-dimensional tantalum photonic crystal absorbers and emitters," Sol. Energy Mater. Sol. Cells **122**, 287–296 (2014).
14. D. O'Connor and A. V. Zayats, "The third plasmonic revolution," Nat. Nanotechnol. **5**(7), 482–483 (2010).
15. N. Zhou, X. Xu, A. T. Hammack, B. C. Stipe, K. Gao, W. Scholz, and E. C. Gage, "Plasmonic near-field transducer for heat-assisted magnetic recording," Nanophotonics **3**(3), 141–155 (2014).
16. S. T. Sundari, S. Chandra, and A. K. Tyagi, "Temperature dependent optical properties of silver from spectroscopic ellip-sometry and density functional theory calculations," J. Appl. Phys. **114**(3), 033515 (2013).
17. H. Reddy, U. Guler, K. Chaudhuri, A. Dutta, A. V. Kildishev, V. M. Shalaev, and A. Boltasseva, "Temperature-dependent optical properties of single crystalline and polycrystalline silver thin films," ACS Photonics **4**(5), 1083–1091 (2017).
18. W. Li, U. Guler, N. Kinsey, G. V. Naik, A. Boltasseva, J. Guan, V. M. Shalaev, and A. V. Kildishev, "Refractory plasmonics with titanium nitride: broadband metamaterial absorber," Adv. Mater. **26**(47), 7959–7965 (2014).
19. L. Braic, N. Vasilantonakis, B. Zou, S. A. Maier, N. M. Alford, A. V. Zayats, and P. K. Petrov, "Optimizing strontium ruthenate thin films for near-infrared plasmonic applications," Sci. Rep. **5**(1), 9118 (2015).
20. J. A. Briggs, G. V. Naik, Y. Zhao, T. A. Petach, K. Sahasrabuddhe, D. Goldhaber-Gordon, N. A. Melosh, and J. A. Dionne, "Temperature dependent optical properties of titanium nitride," Appl. Phys. Lett. **110**(10), 101901 (2017).
21. M. P. Wells, B. Zou, B. G. Doiron, R. Kilmurray, A. P. Mihai, R. F. M. Oulton, P. Gubeljak, K. L. Ormandy, G. Mallia, N. M. Harrison, L. F. Cohen, S. A. Maier, N. McN. Alford, and P. K. Petrov, "Tunable, low optical loss strontium molybdate thin films for plasmonic applications," Adv. Opt. Mater. **5**(22), 1700622 (2017).
22. D. Y. Wan, Y. L. Zhao, Y. Cai, T. C. Asmara, Z. Huang, J. Q. Chen, J. Hong, S. M. Yin, C. T. Nelson, M. R. Motapothula, B. X. Yan, D. Xiang, X. Chi, H. Zheng, W. Chen, R. Xu, A. Ariando, A. Rusydi, A. M. Minor, M. B. H. Breese, M. Sherburne, M. Asta, Q.-H. Xu, and T. Venkatesan, "Electron transport and visible light absorption in a plasmonic photocatalyst based on strontium niobate," Nat. Commun. **8**, 15070 (2017).
23. M. P. Wells, B. Zou, A. P. Mihai, R. Bower, A. Regoutz, S. Fearn, S. A. Maier, N. McN. Alford, and P. K. Petrov, "Multiphase strontium molybdate thin films for plasmonic local heating applications," https://arxiv.org/abs/1803.03131, Date of access: 09 March 2018.
24. P. Patsalas, N. Kalfagiannis, and S. Kassavetis, "Optical properties and plasmonic performance of titanium nitride," Materials (Basel) **8**(6), 3128–3154 (2015).
25. L. Braic, N. Vasilantonakis, A. Mihai, I. J. Villar Garcia, S. Fearn, B. Zou, N. McN. Alford, B. Doiron, R. F. Oulton, S. A. Maier, A. V. Zayats, and P. K. Petrov, "Titanium Oxynitride Thin Films with Tunable Double Epsilon-Near-Zero Behavior for Nanophotonic Applications," ACS Appl. Mater. Interfaces **9**(35), 29857–29862 (2017).
26. G. V. Naik, J. L. Schroeder, X. Ni, A. V. Kildishev, T. D. Sands, and A. Boltasseva, "Titanium nitride as a plasmonic material for visible and near-infrared wavelengths," Opt. Mater. Express **2**(4), 478–489 (2012).
27. M. A. Ordal, R. J. Bell, R. W. Alexander, Jr., L. A. Newquist, and M. R. Querry, "Optical properties of Al, Fe, Ti, Ta, W, and Mo at submillimeter wavelengths," Appl. Opt. **27**(6), 1203–1209 (1988).
28. P. B. Johnson and R. W. Christy, "Optical constants of transition metals: Ti, v, cr, mn, fe, co, ni, and pd," Phys. Rev. B **9**(12), 5056–5070 (1974).
29. M. A. Ordal, L. L. Long, R. J. Bell, S. E. Bell, R. R. Bell, R. W. Alexander, Jr., and C. A. Ward, "Optical properties of the metals al, co, cu, au, fe, pb, ni, pd, pt, ag, ti, and w in the infrared and far infrared," Appl. Opt. **22**(7), 1099–1120 (1983).
30. H. C. Kim, T. L. Alford, and D. R. Allee, "Thickness dependence on the thermal stability of silver thin films," Appl. Phys. Lett. **81**(22), 4287–4289 (2002).
31. G. G. Paulson and A. L. Friedberg, "Coalescence and agglomeration of gold films," Thin Solid Films **5**(1), 47–52 (1970).
32. H. G. Tompkins, "The initial stages of the oxidation of titanium nitride," J. Appl. Phys. **71**(2), 980–983 (1992).
33. W. Li, U. Guler, N. Kinsey, G. V. Naik, A. Boltasseva, J. Guan, V. M. Shalaev, and A. V. Kildishev, "Refractory plasmonics with titanium nitride: broadband metamaterial absorber," Adv. Mater. **26**(47), 7959–7965 (2014).
34. D. Adams, B. A. Julies, J. W. Mayer, and T. L. Alford, "Corrosion of titanium-nitride encapsulated silver films exposed to a H2S ambient," Thin Solid Films **332**(1–2), 235–239 (1998).

Optics EXPRESS

35. M. A. Ordal, R. J. Bell, R. W. Alexander, Jr., L. L. Long, and M. R. Querry, "Optical properties of fourteen metals in the infrared and far infrared: Al, Co, Cu, Au, Fe, Pb, Mo, Ni, Pd, Pt, Ag, Ti, V, and W," Appl. Opt. **24**(24), 4493–4499 (1985).

1. Introduction

Resulting from the resonant oscillations of free electrons within a metallic material upon stimulus by electromagnetic radiation, surface plasmons offer a powerful means of coupling the energy of light to the electrons at metal/dielectric interfaces, breaking the diffraction limit [1,2]. As a result, the field of plasmonics has been extensively researched in recent years with a view to the advancement of technologies such as sub-wavelength imaging [1], communication systems [3], photonics [4] and energy harvesting [5].

Historically the noble metals Au and Ag have formed the basis of plasmonics research. These materials offer several advantages, such as high electrical conductivity [6] and, in the case of Au, good chemical stability [2]. However, they are each subject to a number of practical limitations, such as significant interband transition losses [7], incompatibility with standard CMOS technology [8], and relatively poor thermal stability [2]. The latter has been addressed by providing a thin alumina coating facilitating operation at temperatures in excess of 800° C in atmospheric conditions, however, such an approach prevents direct access to the metal surface, and may therefore hinder applications in areas such as hot electron photochemistry, hot carrier injection into semiconductors and local heating [9]. The strong field confinement characteristic of plasmonic nanostructures inevitably gives rise to high electromagnetic energy densities, and hence the local heating of devices [10]. The resulting lack of thermal stability is particularly detrimental for applications at high temperatures. For example, the area of solar thermophotovoltaics (STPV) stands to benefit significantly from the development of refractory plasmonic metals, offering the potential for energy conversion efficiencies of up to 85% [11,12]. However, in order to achieve such figures there is a need to find new plasmonic materials capable of delivering high absorption over a large frequency range, while withstanding the necessarily high operating temperatures, typically in excess of 730° C [13,14]. Additionally, refractory plasmonic materials are expected to facilitate advances in data storage technology, in particular the development of heat-assisted magnetic recording (HAMR) techniques [15]. Once again, such applications require the thermal stability of materials at high temperatures, as localised heating effects are an integral aspect of the HAMR technique.

While recent research has been conducted into the temperature dependence of the optical properties of Au and Ag thin films, describing their plasmonic performance in vacuum conditions at temperatures up to 500° C and 600° C respectively [10,16,17], data regarding the long term thermal stability of thin films of the refractory materials W, Mo and Ti are scarce. It is also expected that the behaviour of materials experiencing high temperatures in air and in vacuum will be different. Although TiN [18] and, more recently, $SrRuO_3$ (SRO) [19] have been proposed as promising alternative plasmonic materials to Ag and Au owing in part to their refractory properties, experimental research in support of theoretical predictions is severely lacking. The optical properties of TiN have, however, been characterised at elevated temperatures, with the material shown to retain metallic behaviour above 1200° C under vacuum conditions [20]. The perovskite oxides $SrMoO_3$ (SMO) [21] and $SrNbO_3$ (SNO) [22] have also been recently identified as possible alternative plasmonic materials. In the case of SMO, it has been shown that metallic behaviour can be retained up to 700° C [23], subject to deposition conditions, while an equivalent study on SNO is again lacking. This article describes a comparative study of the effects of temperature on the optical and electrical properties of Au, Ag, TiN, TiON, SNO, SMO and SRO, along with known refractory metals Mo, W, and Ti. Experiments are conducted before and after annealing in air at high temperatures for one hour, where the temperature is raised incrementally to a maximum of 1000° C and slow cooled.

Optics EXPRESS

2. Experimental

All samples of Ag and Au were e-beam evaporated in vacuum (10^{-7} mBar) using a Mantis QUAD-EV source with a deposition rate kept at approximately 0.2A/s. A MANTIS deposition system was also used to deposit TiON and TiN by RF reactive magnetron sputtering. Titanium nitride samples were produced at 600° C using 200 W to achieve a deposition rate of 0.15 Å s-1 in 30% N_2 / N_2 + Ar atmosphere. Titanium oxynitride samples were produced at room temperature, again using 200 W to achieve a deposition rate of 0.15 Å s^{-1} in 30% N_2 / N_2 + Ar atmosphere. Ti, Mo and W samples were grown via DC magnetron sputtering at 200°C under an Ar atmosphere. For all samples, the sputtering chamber was pre-baked at 600°C for 2 hours followed by a Ti getter reaction to reduce the residual oxygen partial pressure to below $3x10^{-9}$ mBar. A current of 300 mA was used for Ti and Mo samples and 280 mA for W samples to achieve a deposition rate of 1 Å s^{-1}.

Samples of $SrRuO_3$ and $SrNbO_3$ were prepared via pulsed laser deposition using a KrF excimer laser with a wavelength of 240 nm and pulse duration of 25 ns. The deposition process was conducted with a fluence of approximately 1.7 J cm^{-2} and a repetition rate of 8 Hz. For $SrRuO_3$ an O_2 partial pressure of 50 mTorr was used. Once the deposition was complete, the chamber was filled with O_2 to a pressure of 500 Torr and cooled to 30° C, at which point the sample was removed from the chamber. As with the samples produced by sputtering, the substrate material was double side polished MgO (100) with a surface area of 10 x 10 mm. For $SrNbO_3$, the chamber base pressure was approximately 1×10^{-7} Torr and deposition carried out on $SrTiO_3$ substrate at 800° C. Following the deposition, samples were cooled to 30° C before removal from the chamber.

Samples were annealed in an MTI KSL-1100X-S furnace for 1 hour, the temperature having been raised over the course of 100 minutes. After annealing the samples were cooled to room temperature over a period of 1 hour.

All measurements subsequently conducted on the samples were conducted at room temperature ex-situ. Sample thickness measurements were conducted using a Dektak 150 surface profiler. DC resistivity was measured using the 4-probe technique. The optical constants of each sample were measured by means of ellipsometry. Measurements were conducted using a J. A. Woollam Co. HS-190 ellipsometer at an incident angle of 70°. To extract the data for each material the optical constants of the substrate were considered known, while the properties of the films were fitted to experimental data measured at 65 - 80° according to, where possible, a Drude model with up to 3 Lorentz oscillator terms as described by Eq. (1) [24].

$$\varepsilon(\omega)+i\varepsilon(\omega)=\varepsilon_{\infty}-\frac{\omega_{pu}^2}{\omega^2-i\Gamma_D\omega}+\sum_{j=1}^{m}\frac{f_j\omega_{0j}^2}{\omega_{0j}^2-\omega^2+i\gamma\omega} \quad (1)$$

Here, ω_{pu} denotes the unscreened plasma frequency while the Lorentz oscillator terms are defined in terms f_j, γ_j, and $E_{oj} = \hbar\omega_{oj}$, corresponding to strength, damping factor, and energy respectively. The values determined for each of these parameters are given in the appendix. Where, owing to the degradation of optical properties following annealing treatment, such a model was no longer pertinent, the optical properties of the films were fitted directly to experimental data using the Marquardt minimisation algorithm.

X-ray diffraction measurements were acquired using a Bruker D2 PHASER system with a Cu Kα wavelength of 1.54 Å. A Lake Shore 8400 Hall system was used for AC Hall effect measurements with a field strength of 1.19 T and a current of 15 mA. Four point transport measurements were made to determine the resistivity and Hall components as a function of magnetic field. A single carrier transport model was used to extract carrier concentration and mobility. AFM images were acquired using a Bruker Innova system operating in tapping mode with a scan rate of 1 Hz.

Optics EXPRESS

3. Results and discussion

Samples of Au and Ag were produced via e beam evaporation, samples of W, Mo and Ti, via RF magnetron sputtering and TiN samples via RF reactive magnetron sputtering on (100) oriented MgO and Si substrates. Additionally, epitaxial SNO and SRO samples were produced using pulsed laser deposition (PLD), with $SrTiO_3$ (100) and MgO (100) used respectively as substrate materials. The thicknesses of TiN, TiON, Au, and Ag samples were found to be 50 ± 5 nm and SNO and SRO samples were measured as 105 ± 5 nm, and 95 ± 5 nm respectively. Samples of W, Mo and Ti were 80 ± 5 nm, with thicker samples having been produced to avoid surface oxidation dominating the measured optical and electrical properties. The XRD data for each material are provided and discussed in the appendix. The films were grown on both MgO and Si substrates and the as grown film quality was found to be rather insensitive to the substrate type, though minor variations in the values of Re(ε) and Im(ε) were found to result from the change of substrate. For simplicity the analysis is confined to films grown on MgO. However, it should be noted that Au was found to diffuse into the Si upon heating, further details of which can be found in the appendix.

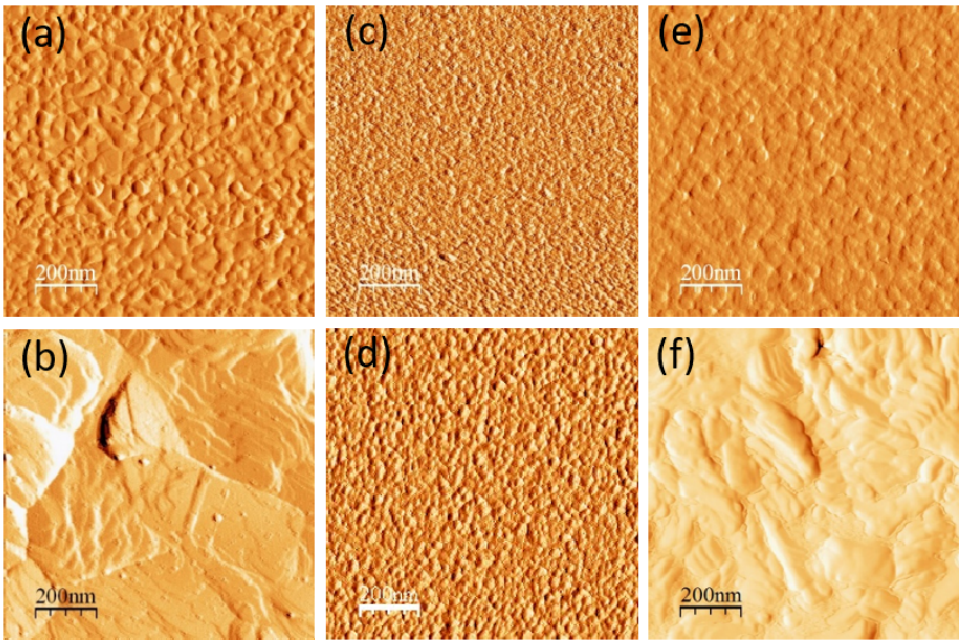

Fig. 1. AFM images showing (a) Au before annealing, (b) Au after annealing at 600° C, (c) TiON before annealing, (d) TiON after annealing at 500° C, (e) W before annealing, (f) W after annealing at 500° C

Figure 1 shows examples of the AFM images before and after the anneal. The RMS roughness values for each sample are summarised in Table 1 (note that samples of Au, Ag, TiN and TiON were measured over a 10 x 10 μm^2 area, while all other samples were measured over a 1 x 1 μm^2 area). By the 500° C anneal most films show significant topographic changes and enhanced roughness, while there is also a systematic increase in the roughness of the films after annealing at higher temperatures. For TiON and TiN, the increase in surface roughness is much less pronounced than the other films.

Optics EXPRESS

Table 1. Changes in surface roughness with annealing temperature (Au, Ag, TiN and TiON measured over a 10 x 10 µm^2 area, Ti, Mo, W, SRO and SNO were measured over a 1 x 1µm^2 area)

Annealing Temperature (° C)	RMS - Surface Roughness (nm)								
	Ti	Mo	W	Ag	Au	TiN	TiON	SRO	SNO
-	7.4	2.5	1.1	2.4	1.2	0.7	0.7	1.4	0.2
300	6.9	1.6	1.5	Not continuous	0.9	0.7	0.7	4.4	0.4
400	4.5	7.0	0.8	-	0.7	0.5	0.5	7.5	0.5
500	2.9	8.5	10.3	-	0.5	2.8	2.9	-	-
600	-	-	-	-	1.9	-	-	-	-
800	-	-	-	-	-	-	-	15.1	-
1000	-	-	-	-	-	-	-	43.9	-

Figure 2 depicts the real and imaginary components of the dielectric permittivity for the noble metals, Au and Ag. Figures 3-5 meanwhile describe the dielectric permittivity for the pure metals, Ti, Mo and W, for the metallic compounds, TiN and TiON, and the perovskite oxides SNO, SMO and SRO respectively. It should be noted that optical data for SMO were taken from [23], and are provided for comparative purposes only.

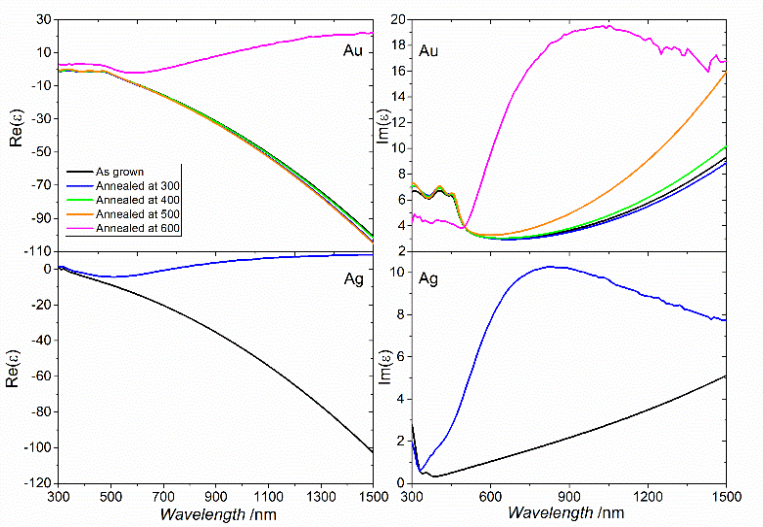

Fig. 2. Ellipsometry data showing real and imaginary parts of the dielectric permittivity for samples of Ag and Au after annealing at temperatures from 300 - 600° C

Optics EXPRESS

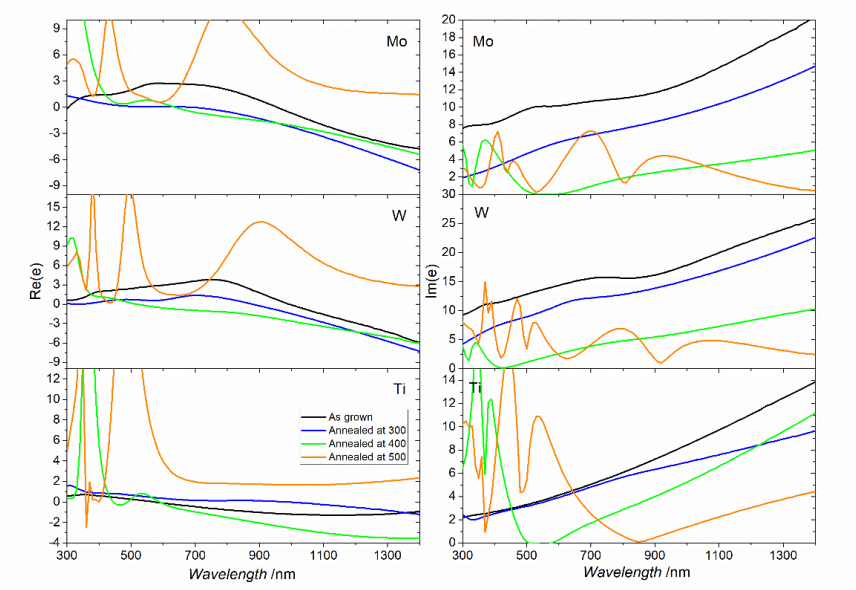

Fig. 3. Ellipsometry data showing real and imaginary parts of the dielectric permittivity for samples of Mo, W, and Ti after annealing at temperatures from 300 - 500° C

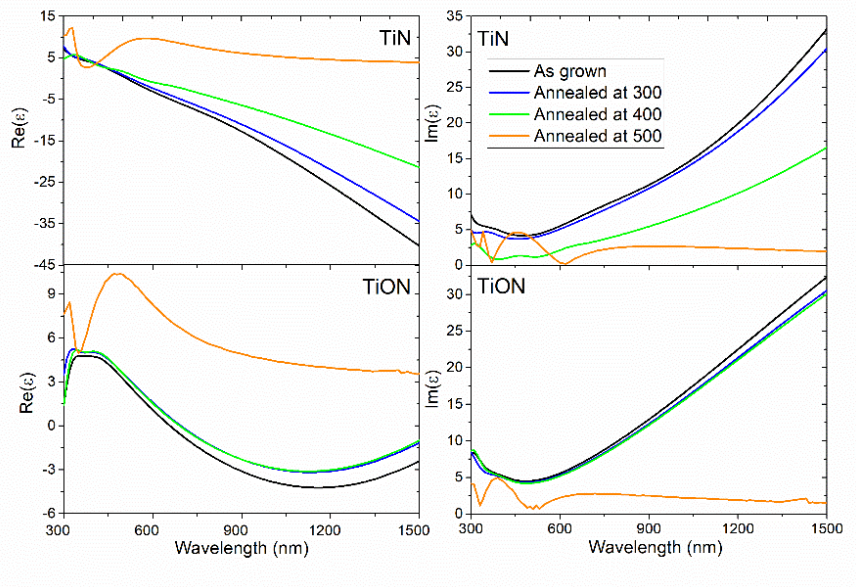

Fig. 4. Ellipsometry data showing real and imaginary parts of the dielectric permittivity for samples of TiN, TiON and SRO after annealing at temperatures from 300 - 500° C

Optics EXPRESS

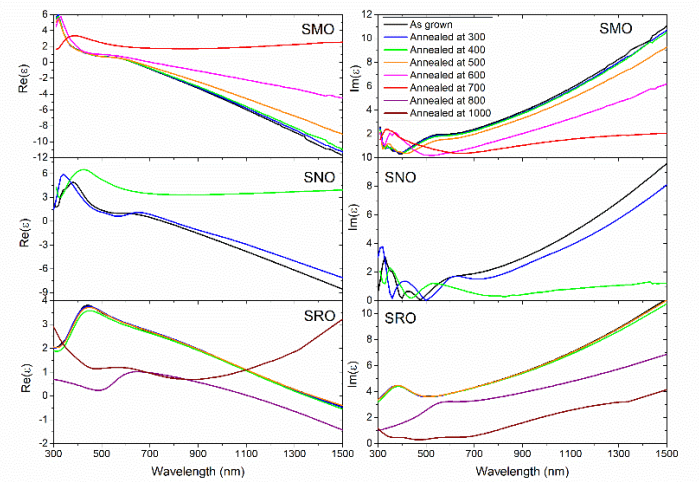

Fig. 5. Ellipsometry data showing real and imaginary parts of the dielectric permittivity for samples of SMO (from [23]), SNO and SRO after annealing at temperatures from 300 - 1000° C

Each of the four figures shows the results of measurements taken before and after annealing in air for 1 hour at temperatures between 300 and 1000° C. The optical data show a loss of metallic behaviour for each material. It should be noted that the pre-anneal room temperature optical measurements of Ag, Au, TiN, TiON, SNO and SRO [7,10,19,22,24–26] are found to be in agreement with previous studies. In the case of TiN however, it is well known that the optical properties are heavily dependent upon deposition conditions, and may be noted consequently that TiN of a more metallic nature has been more recently reported [20]. Additionally, the effects of temperature on the optical properties of Au appear consistent with the findings of Reddy et al [10]. However, in the case of TiN, the trends observed in the imaginary part of the dielectric permittivity are found to oppose those reported by Briggs et al. [20], while we find a transition to dielectric behaviour after annealing at 500° C which is in contrast to the high temperature stability (in excess of 1200° C) recorded by Briggs et al., where samples were heated under vacuum conditions. Meanwhile, both real and imaginary parts of the dielectric permittivity for samples of Ti, W, and Mo are found to be smaller in magnitude than those of reference data as a result of their propensity to oxidation, both during growth and upon removal from the vacuum chamber [27,28]. There is a correlation between the optical properties and the changes in the DC electrical resistivity, summarised in Table 2. Films annealed at high temperature show an increase in electrical resistivity.

Table 2. Changes in DC resistivity with annealing temperature

Annealing Temperature (° C)	Resistivity (μΩ cm)								
	Ti (± 15%)	Mo (± 15%)	W (± 15%)	Ag (± 15%)	TiN (± 5%)	TiON (± 5%)	Au (± 20%)	SRO (± 10%)	SNO (± 10%)
-	562	98	149	2.5	170	272	4.2	527	30
300	917	123	196	∞	177	295	3.6	590	99
400	975	145	182		204	285	5.7	518	∞
500	∞	∞	5610		∞	∞	3.7	514	
600							∞	-	
800								569	
1000								∞	

Although the electrical behaviour of Ag, Au and SRO can be considered primarily a result of morphological changes, the electrical behaviour of TiN, TiON, and SRO, were considered

Optics EXPRESS

in part a result of changes to the fundamental properties of the materials. Consequently, the electrical properties were examined in more detail, in particular, the changes in carrier concentration and mobility were extracted from Hall measurements, in combination with longitudinal resistivity, as a function of anneal history. These results are summarised in Table 3.

Table 3. Changes in charge carrier dynamics due to annealing

	TiN		TiON		SRO	
	Room temperature	After annealing at 400° C	Room temperature	After annealing at 400° C	Room temperature	After annealing at 800° C
Charge carrier density (cm^{-3})	$6x10^{22}$ ± $3 x10^{22}$	$1x10^{22}$ ± $5 x10^{21}$	$2x10^{21}$ ± $6 x10^{20}$	$8x10^{20}$ ± $4 x10^{14}$	$6x10^{22}$ ± $3 x10^{22}$	$4x10^{22}$ ± $2 x10^{22}$
Charge carrier mobility ($cm^2 V.s^{-1}$)	0.8 ± 0.3	1.8 ± 0.7	7.8 ± 1.5	6.3 ± 1.3	0.1 ± 0.03	0.1 ± 0.03

The real and imaginary components of dielectric permittivity are described by the Drude equation [29], where ε_∞ refers to the background dielectric constant, ω_p to the plasma frequency, and Γ_D to the Drude broadening.

$$\varepsilon'(\omega) + i\varepsilon''(\omega) = \varepsilon_\infty - \frac{\omega_p^2}{\omega^2 + i\Gamma_D\omega} \tag{2}$$

For a perfectly free electron gas ε_∞ may be assumed to be approximately equal to 1. Therefore, Eq. (2) may be separated into real and imaginary parts described by Eqs. (3) and (4).

$$\varepsilon'(\omega) \approx 1 - \frac{\omega_p^2}{\Gamma_D^2 + \omega^2} \tag{3}$$

$$\varepsilon''(\omega) \approx \frac{\Gamma_D \omega_p^2}{\omega^3} \tag{4}$$

It should be noted that the above Drude model, although a reasonable model for Au and Ag in the upper visible and near-IR, does not account for the effects of interband transitions, and so is used here solely for descriptive purposes, however the ellipsometry data shown in Figs. 2-5 were fitted using a Drude model with up to 3 Lorentz oscillator terms. The plasma frequency of a material is directly proportional to the charge carrier density, N, though inversely proportional to the effective mass, m*.

The Drude broadening is determined by electron – electron scattering, electron – phonon scattering, and surface scattering effects. An increase in surface roughness and, resultantly, in surface scattering effects may also increase Γ_D.

It can be seen from Table 1 and Fig. 2 that Ag and Au behave similarly, with both real and imaginary parts of ε increasing greatly above a given threshold temperature. In Au, it can also be seen that an increase in surface roughness accompanies this behaviour, resulting from the increase in temperature [10], and so accounting for an increase in the surface scattering effects represented by Γ_D. From Eqs. (3) and (4) it can be seen that an increase in Drude broadening will increase both ε' and ε''. Kim et al. [30] report that the resistivity of Ag becomes infinite above a given threshold temperature as a result of the agglomeration of the thin-film leading to a loss of film continuity. Furthermore, a thickness dependence of this threshold temperature is observed, with their results suggesting the cut-off temperature for a 50 nm Ag film to be in the region of 200° C. It should also be noted that Ag is well known for

Optics EXPRESS

its propensity to oxidation and sulfidation even under atmospheric conditions, however, although the XRD spectra in the appendix (Fig. 10) show a degree of oxidation of the film, such effects are found to be less significant than those of the surface agglomeration to the degradation of the optical properties, as AFM measurements show a loss of continuity in the film. The results of Paulson et al. show that the degradation of Au can be understood in the same way [31]. The data presented here are consistent with these observations.

Although the refractory properties of Ti, W, and Mo are well reported in the case of bulk materials, Fig. 3 shows the optical properties of thin-film samples are subject to significant variations at relatively low temperatures, with metallic behaviour being lost altogether after annealing in air at 500° C. In the case of Mo this can simply be attributed to oxidation, as confirmed by XRD measurements. By contrast, Ti and W are shown to undergo more significant morphological changes, as highlighted by Table 1. Furthermore, XRD measurements confirm the oxidation of the samples, along with a loss of the crystalline metallic phases, leading to the observed loss of metallic behaviour.

TiN has been claimed as a good alternative material to the noble metals owing in part to its superior thermal stability [18]. Here however, changes are present in both ε' and ε" after annealing in air at 300° C. The kinetics of the oxidation of TiN have previously been described by H. G. Tompkins [32], who identifies an increasing rate of oxidation in TiN thin films as temperatures are increased above 350° C, in apparent agreement with these results. It may further be noted that the trends observed for ε' and ε" in this case oppose each other, as ε' consistently increases with temperature, while ε" decreases. As a result, it may be reasoned that the changes in optical properties arise predominantly from variations in ω_p rather than in Γ_D. This statement is supported by AC Hall effect measurements which show a decrease of a factor of 6 in the charge carrier concentration and an increase from 0.8 to 1.8 $cm^2\ V.s^{-1}$ in charge carrier mobility upon annealing at 400° C. These changes may be expected to have the respective effects of raising and decreasing ω_p, however as the magnitude of the change in carrier concentration is significantly larger than that of carrier mobility, this appears as the dominant factor. After annealing at 500° C there is an increase in surface roughness which may be attributed to oxidation.

Such results appear contradictory to those presented by Li et al., who demonstrate that, in the context of a metamaterial absorber, the physical shape and optical performance of TiN remain unchanged after heating to 800° C for 8 hours, while the same conditions are sufficient to melt Au [33]. Moreover, Briggs et al. show that TiN retains metallic behaviour in the visible regime up to temperatures in excess of 1200° C [20]. However, while the samples measured here were annealed in air, those of Li et al. and Briggs et al. were annealed under vacuum conditions. Operation under vacuum limits the widespread applicability of TiN unless suitable encapsulation materials are utilized; only under these conditions might one conclude that TiN is attractive for high temperature applications. These results further highlight the limitations of the use of TiN itself as an encapsulation layer, as studied by Adams et al [34].

TiON can be seen to exhibit similar variations due to temperature as TiN. However, greater stability is observed between annealing temperatures of 300 and 400° C, and may be attributed to the fact the material is already partially oxidised. AC Hall effect measurements also show an improvement in stability, with charge carrier concentration changing only from $2x10^{21}$ to $9x10^{20}$ cm^{-3} and mobility from 7.8 to 6.4 $cm^2\ V.s^{-1}$. It may be noted that the decrease in charge carrier mobility here opposes the trend observed in TiN, however this difference may be accounted for by the error margins of each measurement.

The optical properties of SRO exhibit little change following annealing at temperatures below 800° C. However, after annealing at 800° C, variations are observed with both ε' and ε" showing the same trend. This indicates the dominance of Γ_D in the behaviour, in contrast to TiN. This is supported by AC Hall effect measurements, which indicate that the charge carrier concentration remains approximately constant within the margins for error, decreasing from

Optics EXPRESS

$5.5x10^{22}$ to $4.3x10^{22}$ cm^{-3} while mobility remains at 0.1 cm^2 $V.s^{-1}$. After annealing at 1000° C a significant increase in ε' is observed along with a decrease in ε", suggesting ω_p to be the dominant variable; however, the large increase in surface roughness observed after this treatment may be expected to have the effect of increasing Γ_D. Indeed, it should be noted that the increase in surface roughness here is of a similar order to that of Au, as opposed to the less significant increase observed for TiN and TiON. Additionally, XRD measurements show the disappearance of peaks corresponding to (100) and (200) crystal orientations after annealing at 1000° C. It may therefore be concluded that structural and morphological changes following annealing at 1000° C result in the degradation of the optical properties of SRO, rather than oxidation, and so similar behaviour may be expected under vacuum conditions.

Figure 5 also shows that SNO, in contrast to SRO, loses metallic behaviour after annealing at 400° C in spite of little variation being observed in the optical properties at lower temperatures. From XRD measurements taken before and after annealing (shown in Fig. 15), this is found to be a result of a phase transition from metallic $SrNbO_3$ to the dielectric $Sr_2Nb_2O_{3.5}$.

As noted previously, although a Drude model constitutes the basis for much of the above analysis, a Drude-Lorentz model was used for the fitting of the ellipsometry data, the parameters of which can be found in the Appendix (Table 4). Qualitatively, the variations in ω_{pu} and Γ_D presented in Table A1 are found to be in agreement with the previous analysis.

Finally, Fig. 6 provides an overview of the operational limits for each of the materials under investigation. The observed maximum operating temperature in air (i.e. the annealing temperature after which metallic behaviour was lost) for each material is plotted against the plasma frequency as reported in literature [19,21,22,23,24,35]. In general, it appears oxide materials such as SRO exhibit superior stability in air than the pure metals and TiN, subject to the absence of any phase transitions as observed in SNO. Further research is therefore recommended into equivalent characterisations of other transition metal nitrides, as well as an analysis of oxide materials under vacuum conditions, analogous to the work of Briggs et al [20].

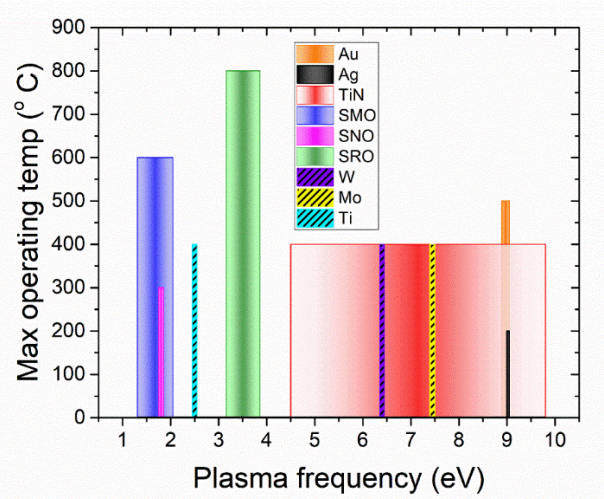

Fig. 6. Figure showing the proposed operating regimes for the materials under study. The temperature at which each material is found to lose metallic behavior due to annealing in air is plotted against the plasma frequencies previously reported for Au [35], Ag [35], TiN [24], SMO [21,23], SNO [22], SRO [19], W [35], Mo [35] and Ti [35].

Optics EXPRESS

4. Conclusion

In summary, thin-film samples of nine materials, namely W, Mo, Ti, TiN, TiON, Ag, Au, SNO and SRO, have been produced through a combination of RF magnetron sputtering, RF reactive magnetron sputtering, and PLD in order to investigate their potential usage in high-temperature plasmonic applications. The optical data from recent comparable experiments on SMO are also included for the purpose of comparison. Measurements of the optical and electrical properties of each sample have found thin films of the commonly reported refractory materials W, Mo and Ti difficult to produce reliably, owing to the apparent influence of surface oxides. Meanwhile, the real part of the dielectric permittivity of Au was found to be stable up to 500° C when deposited on MgO, though the optical losses increased gradually with annealing temperature. After annealing at 600° C, significant changes to the morphology of the Au film were shown to result in a loss of connectivity across the film.

The optical properties of both TiN and TiON have been observed to change significantly upon annealing in air before a loss of metallic behaviour after annealing at 500° C. However, unlike the noble metals, changes to the material properties appear a result of oxidation rather than changes to the surface morphology. It may therefore be concluded that, while Au may be more suitable for high temperature applications in air, TiN and TiON are better suited to high temperature applications operating under vacuum conditions or after suitable protective capping layers are identified. Finally, the optical properties of SNO and SRO are considered, with the results showing that metallic behaviour is lost in SNO after annealing at 400° C due to a phase transition, while being retained in SRO after annealing at 800° C. However, the degradation above this temperature appears a result of the agglomerate formation of the film. Therefore, although SRO may be an attractive alternative to Au for some high temperature applications (if the latter lacks an alumina coating) [9], TiN and TiON may be expected to exhibit superior thermal stability in an encapsulated environment.

Appendix

The XRD data for samples of Mo, W, Ti, TiN, Au, Ag, $SrNbO_3$ (SNO) and $SrRuO_3$ (SRO) are provided below in Figs. 7–16. Samples of Mo and W show no impurity phases in the as deposited films, however after annealing at 500° C it is clear in both cases that the samples have oxidised. By contrast, the data for Ti show the film to become amorphous after annealing, with the intensity of the Ti (200) peak almost completely diminished.

Oxide peaks are noted in the Ag films both before and after annealing at 300° C, however it is only after annealing that a loss of metallic behaviour is observed, as shown by the DC resistivity measurements, presented in Table 2 (see main article).

Au was deposited onto substrates of both Si and MgO and in both cases, as was the case with Ag, some oxide peaks are observed, though these show little effect on the optical and electrical properties of the samples. It should be noted however that the Au (200) peak observed for the sample deposited on Si was no longer present after annealing at 300° C, while the sample deposited on MgO showed no structural changes following the same treatment. Furthermore, additional peaks are observed after annealing on Si which are attributed to the formation of Au-Si composites. This result shows once again the need for alternative plasmonic materials, owing to the incompatibility between Au and Si.

For samples of TiN and TiON the XRD data show no structural changes before and after annealing at 300° C, however it may be noted that the TiN (200) peak observed in both materials is significantly less intense in the TiON sample. Figure 15 shows that, although SNO grows epitaxially on STO, after annealing at 400° C SNO there is a phase transition from $SrNbO_3$ to $Sr_2Nb_2O_{3.5}$. The XRD data for SRO show the presence of additional phases in the film as deposited, such as RuO_2 (310), though more significantly indicate the significant structural changes resulting from annealing at 1000° C through the loss of SrRuO3 (100), (110) and (200) peaks.

Optics EXPRESS

Figures 17–24 show AFM images for samples of Mo, W, Ag, TiON, Au, SNO and SRO both before and after annealing, thereby showing in all cases the clear structural degradation of samples following high temperature exposure.

Finally, Table 4 details the parameters determined from spectroscopic ellipsometry measurements according to a Drude-Lorentz model. In each case the mean squared error (MSE) of the fit was found to be below 30.

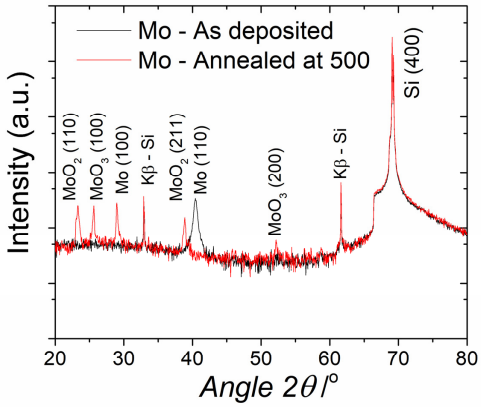

Fig. 7. XRD patterns of Mo sample as deposited on Si and after annealing at 500° C

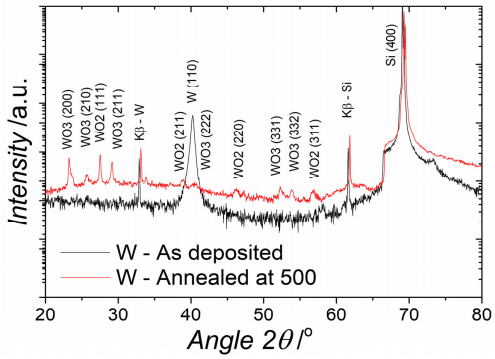

Fig. 8. XRD patterns of W sample as deposited on Si and after annealing at 500° C

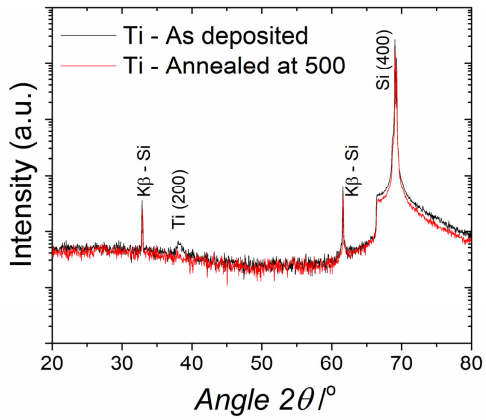

Fig. 9. XRD patterns of Ti sample as deposited on Si and after annealing at 500° C

Optics EXPRESS

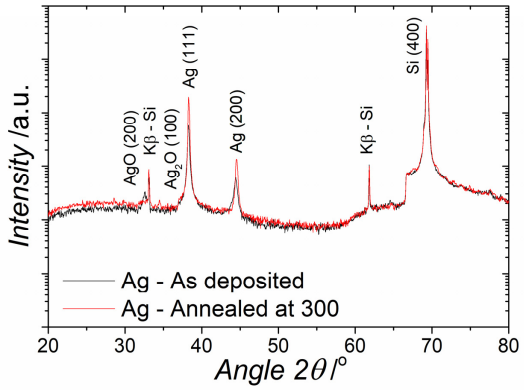

Fig. 10. XRD patterns of Ag sample as deposited on Si and after annealing at 300° C

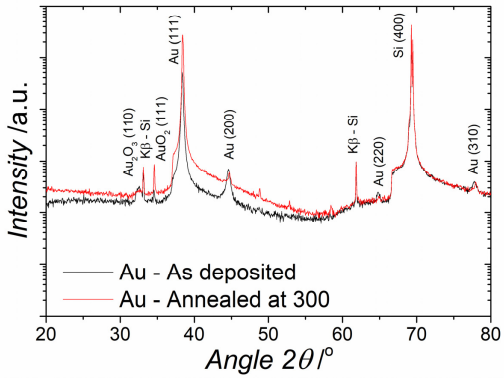

Fig. 11. XRD patterns of Au sample as deposited on Si and after annealing at 300° C

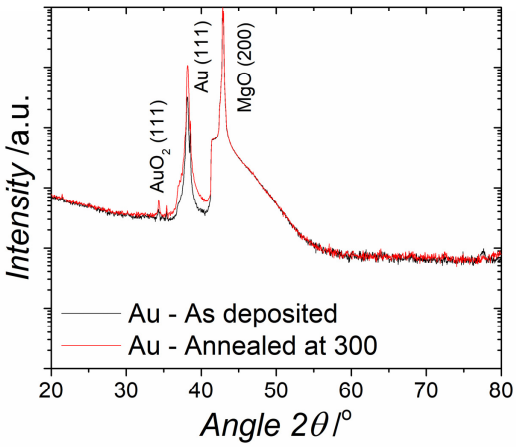

Fig. 12. XRD patterns of Au sample as deposited on MgO and after annealing at 300° C

Optics EXPRESS

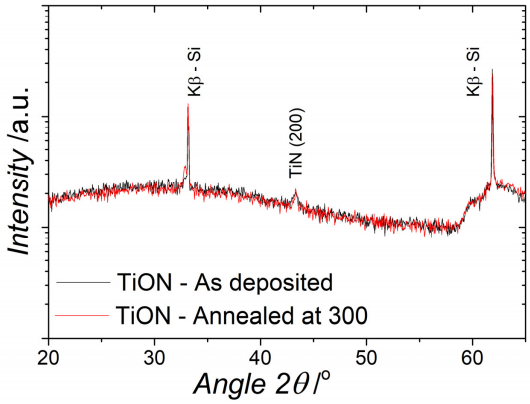

Fig. 13. XRD patterns of TiON sample as deposited on Si and after annealing at 300° C

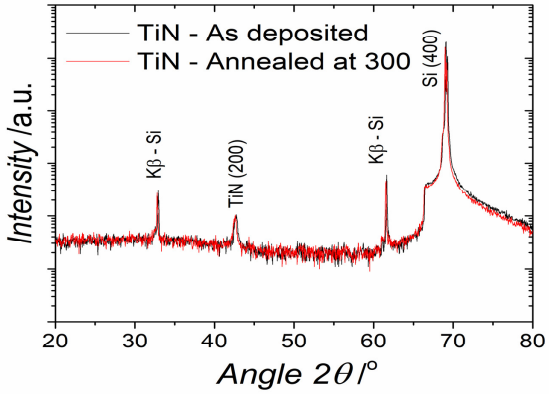

Fig. 14. XRD patterns of TiN sample as deposited on Si and after annealing at 300° C

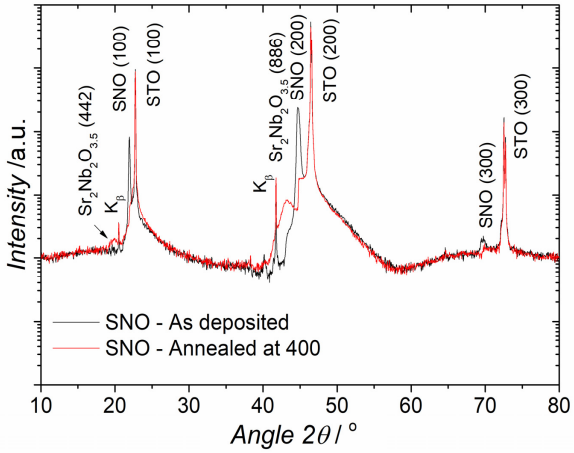

Fig. 15. XRD patterns of SNO sample as deposited on STO and after annealing at 400° C

Optics EXPRESS

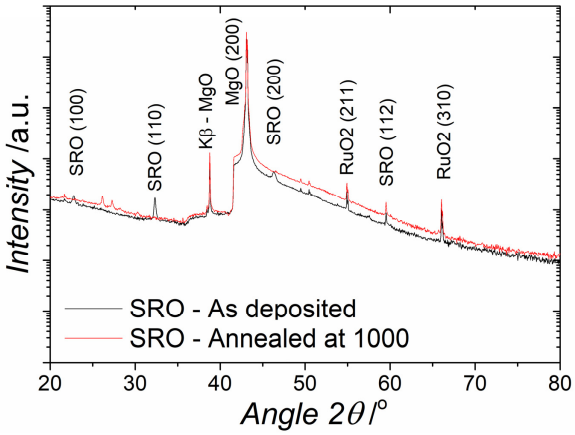

Fig. 16. XRD patterns of SRO sample as deposited on MgO and after annealing at 1000° C

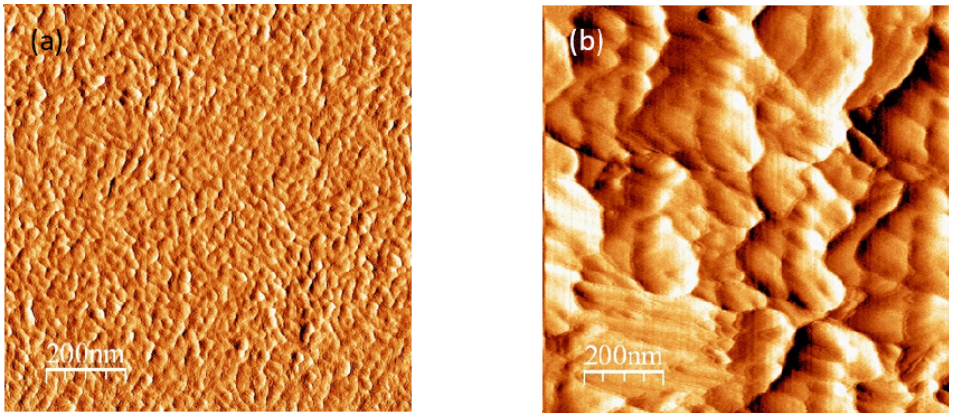

Fig. 17. AFM images of Mo at (a) room temperature and (b) after annealing at 500° C

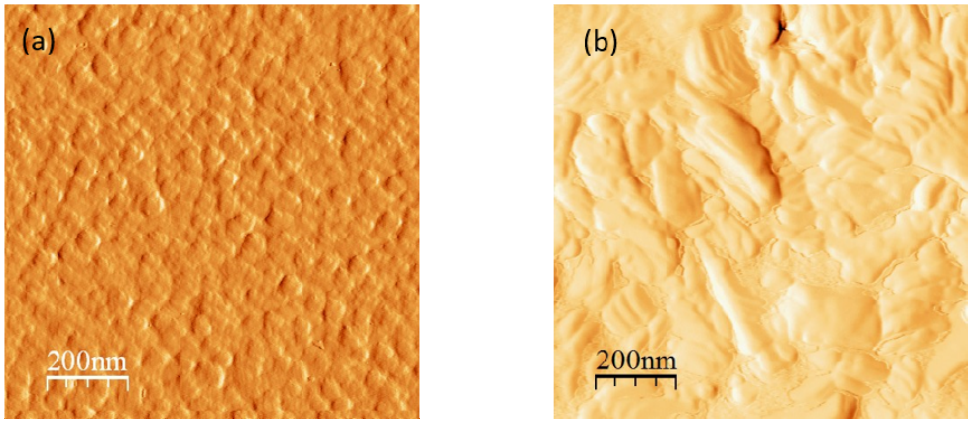

Fig. 18. AFM images of W at (a) room temperature and (b) after annealing at 500° C

Optics EXPRESS

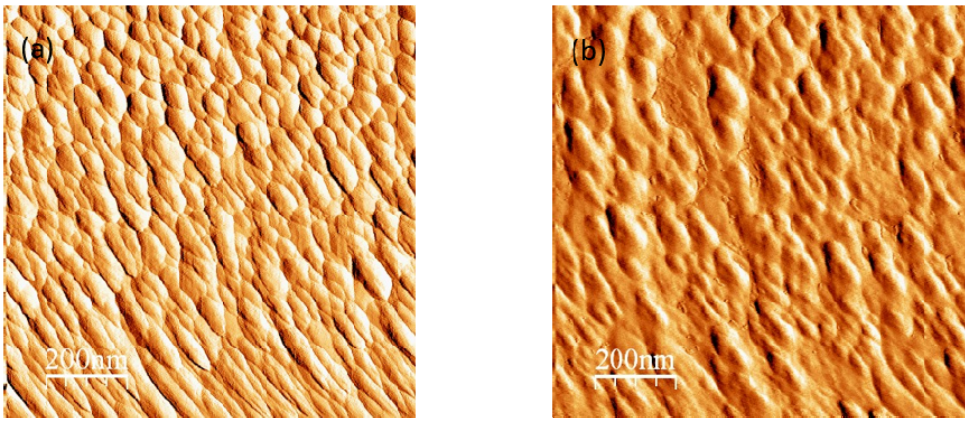

Fig. 19. AFM images of Ti at (a) room temperature and (b) after annealing at 500° C

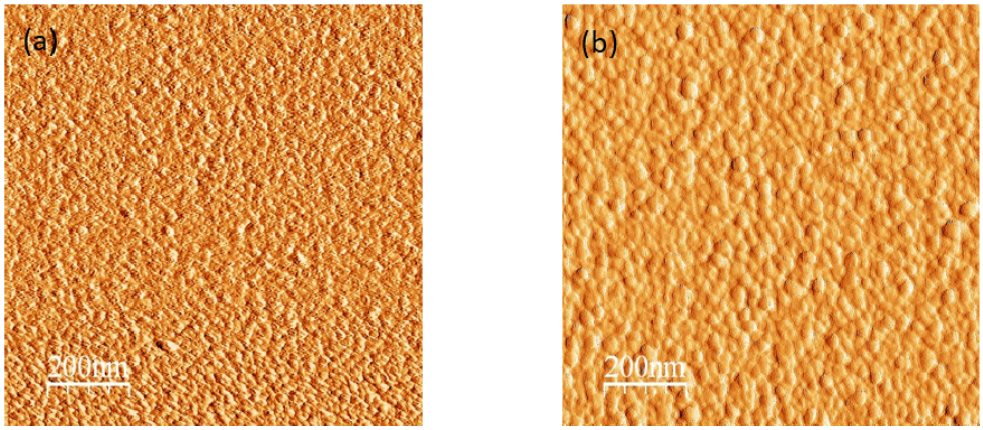

Fig. 20. AFM images of TiON at (a) room temperature and (b) after annealing at 400° C

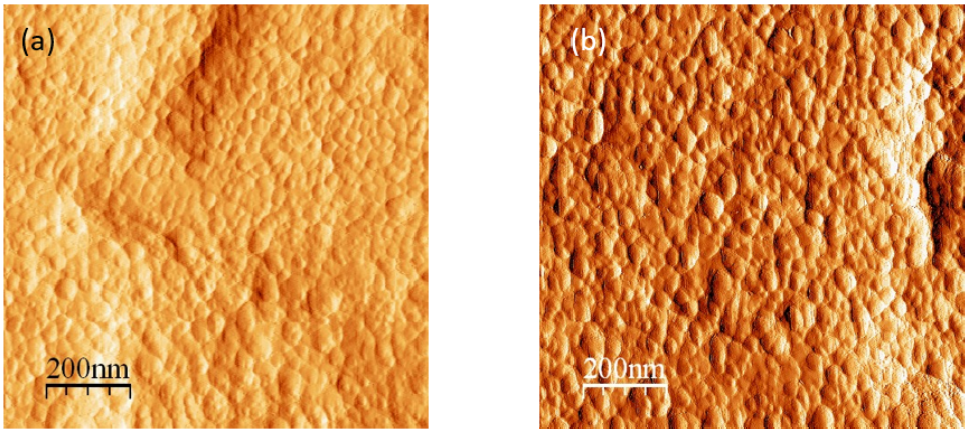

Fig. 21. AFM images of TiN at (a) room temperature and (b) after annealing at 400° C

Optics EXPRESS

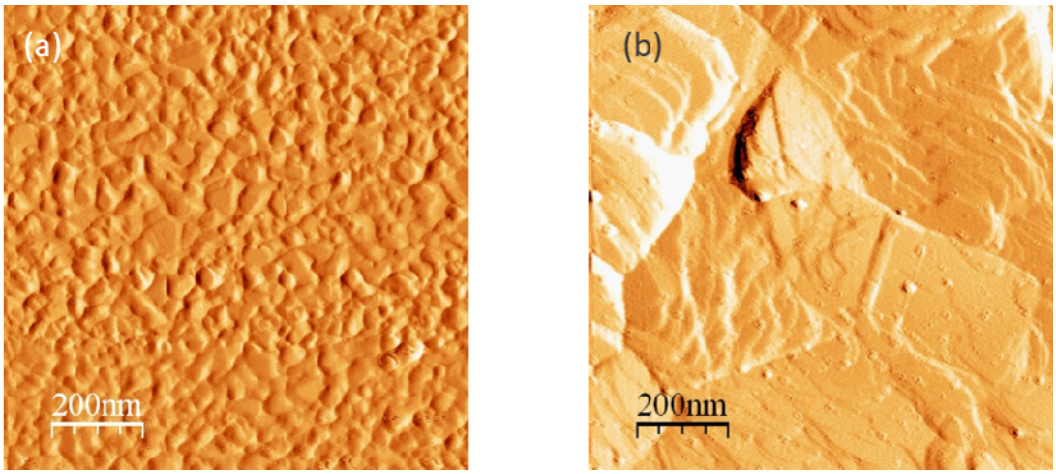

Fig. 22. AFM images of Au at (a) room temperature and (b) after annealing at 600° C

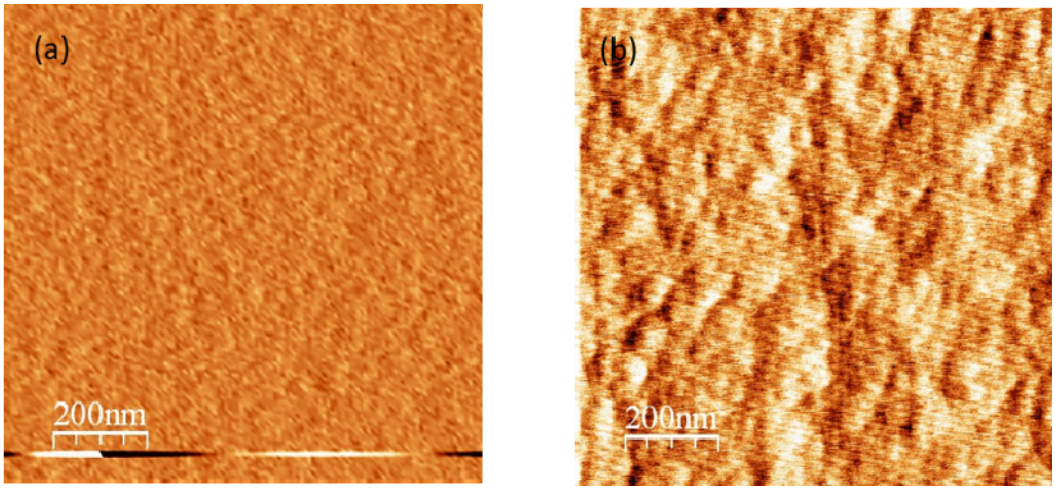

Fig. 23. AFM images of SNO at (a) room temperature and (b) after annealing at 300° C

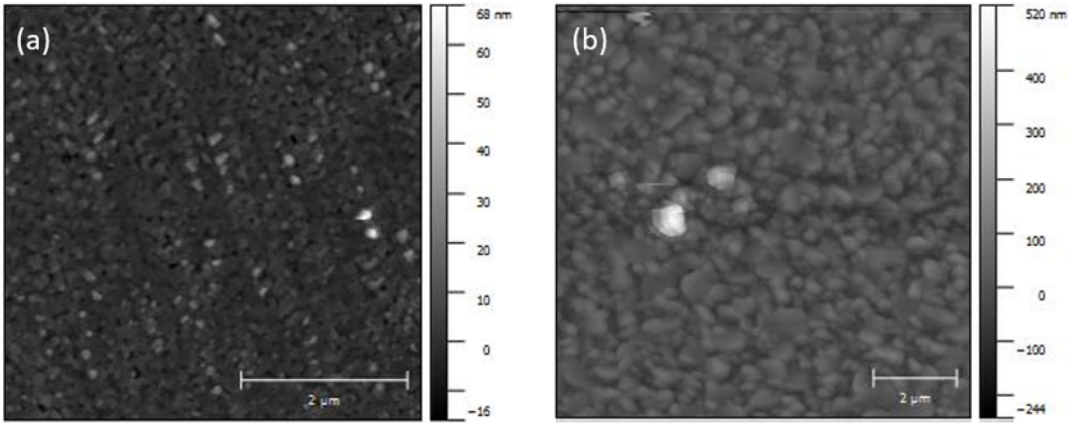

Fig. 24. AFM images of SRO after annealing at (a) 300 and (b) 1000° C

Optics EXPRESS

Table 4. Drude-Lorentz fitting parameters

	T [°C]	ε_{inf}	ω_{pu} [eV]	Γ_D [eV]	ω_{o1} [eV]	ω_{p1} [eV]	Γ_2 [eV]	ω_{o2} [eV]	ω_{p2} [eV]	Γ_2 [eV]	ω_{o3} [eV]	ω_{p3} [eV]	Γ_3 [eV]	MSE
Au	20	1.12	8.17	0.043	2.72	1.44	0.29	3.10	8.39	0.82	5.50	56.75	2.39	0.92
	300	1.12	8.27	0.044	2.75	1.79	0.32	3.13	5.94	0.69	5.07	21.43	0.86	1.45
	400	1.43	7.26	0.054	2.74	1.50	0.28	3.10	5.41	0.64	5.06	22.60	0.99	1.36
	500	1.96	6.26	0.089	2.73	2.15	0.26	3.19	11.13	0.76	4.46	64.02	1.49	1.77
Ag	20	0.87	9.50	0.023	4.65	18.28	0.63	12.70	302.5	5.73	-	-	-	0.65
Ti	20	1.19	3.87	2.53	4.14	25.29	3.72	5.69	7.80	0.001	-	-	-	7.07
	300	3.54	1.87	1.61	2.37	18.93	2.41	3.89	65.24	11.19	-	-	-	1.80
Mo	20	0.43	7.14	0.67	2.37	35.44	2.59	6.98	339.1	0.987	3.75	1.77	0.62	0.79
	300	2.31	2.45	0.39	2.11	7.86	1.71	616.1	77.62	8.59	-	-	-	17.54
W	20	2.08	4.39	6.57	4.23	98.13	3.65	0.43	6.99	0.001	2.05	6.42	0.98	15.14
	300	2.32	4.39	4.34	5.54	35.50	1.84	0.10	11.45	0.20	1.93	3.56	0.76	26.90
TiN	20	0.80	7.61	0.39	5.37	179.7	2.21	1.73	3.57	1.15	-	-	-	1.02
	300	0.79	7.22	0.38	5.45	170.6	1.62	1.73	6.33	1.99	-	-	-	1.61
	400	0.79	5.70	0.26	5.98	140.3	0.47	1.95	1.08	0.63	-	-	-	0.81
TiON	20	4.01	2.86	1.14	4.10	44.52	1.38	-	-	-	-	-	-	6.50
	300	3.96	2.79	1.14	4.29	51.15	1.46	-	-	-	-	-	-	19.92
	400	4.04	2.74	1.15	4.09	42.07	1.23	-	-	-	-	-	-	4.89
SNO	20	3.77	1.71	0.48	1.64	4.38	4.09	3.79	4.01	0.40	-	-	-	3.69
	300	3.81	1.57	0.51	1.30	0.26	0.54	3.54	1.83	1.92	-	-	-	7.88
SRO	20	1.78	2.11	0.48	3.05	82.20	19.51	3.35	14.79	1.76	-	-	-	1.33
	300	1.78	2.00	0.48	2.92	73.72	17.57	3.36	14.87	1.77	-	-	-	1.46
	400	1.78	2.00	0.46	2.31	40.19	9.50	3.33	14.58	1.74	-	-	-	0.86
	500	1.78	2.00	0.49	2.65	57.77	13.80	3.33	14.57	1.74	-	-	-	0.66
	800	1.27	2.01	0.24	3.25	69.78	14.55	2.49	2.48	0.94	-	-	-	0.38

Funding

Engineering and Physical Sciences Research Council (EPSRC) Reactive Plasmonics Programme (EP/M013812/1); Henry Royce Institute through EPSRC grant EP/R00661X/1.

Acknowledgments

P.K.P. and A.P.M. conceived and designed the research. M.P.W., G.G., R.K. R.B. and A.P.M carried out the experiments. All authors contributed to the manuscript writing and agreed on its final contents. S.A.M. further acknowledges the Lee-Lucas Chair.

82.216.208.144 {ts '2019-12-13 08:10:57'}